Cell and Tissue Research (2019) 376:233–245
https://doi.org/10.1007/s00441-018-2971-2

REGULAR ARTICLE

Human umbilical cord blood mesenchymal stem cells expansion via human fibroblast-derived matrix and their potentials toward regenerative application

Se Young Van[1] · Yong Kwan Noh[1,2] · Seong Who Kim[3] · Yeon Mok Oh[4] · Ik Hwan Kim[2] · Kwideok Park[1,5]

Received: 23 May 2018 / Accepted: 23 November 2018 / Published online: 4 January 2019

Abstract

Large expansion of human mesenchymal stem cells (MSCs) is of great interest for clinical applications. In this study, we examine the feasibility of human fibroblast-derived extracellular matrix (hFDM) as an alternative cell expansion setting. hFDM is obtained from decellularized extracellular matrix (ECM) derived from in vitro cultured human lung fibroblasts. Our study directly compares conventional platforms (tissue culture plastic (TCP), fibronectin (FN)-coated TCP) with hFDM using umbilical cord blood-derived MSCs (UCB-MSCs). Early cell morphology shows a rather rounded shape on TCP but highly elongated morphology on hFDM. Cell proliferation demonstrates that MSCs on hFDM were significantly better compared to the others in both 10 and 2% serum condition. Cell migration assay suggests that cell motility was improved and a cell migration marker CXCR4 was notably up-regulated on hFDM. MSCs differentiation into osteogenic lineage on hFDM was also very effective as examined via gene expression, *von Kossa* staining and alkaline phosphatase activity. In addition, as the MSCs were expanded on each substrate, transferred to 3D polymer mesh scaffolds and then cultivated for a while, the data found better cell proliferation and more CXCR4 expression with MSCs pre-conditioned on hFDM. Moreover, higher gene expression of stemness and engraftment-related markers was noticed with the hFDM group. Furthermore when UCB-MSCs expanded on TCP or hFDM were injected into emphysema (a lung disease) animal model, the results indicate that MSCs pre-conditioned on hFDM (with 2% serum) retain more advanced therapeutic efficacy on the improvement of emphysema than those on TCP. Current works demonstrate that compared to the conventional platforms, hFDM can be a promising source of cell expansion with a naturally derived biomimetic ECM microenvironment and may find some practical applications in regenerative medicine.

Keywords Extracellular matrix (ECM) · Human fibroblast-derived matrix (hFDM) · Umbilical cord blood-derived mesenchymal stem cells (UCB-MSCs) · MSCs expansion · Emphysema

Se Young Van and Yong Kwan Noh contributed equally to this work.

Electronic supplementary material The online version of this article (https://doi.org/10.1007/s00441-018-2971-2) contains supplementary material, which is available to authorized users.

✉ Ik Hwan Kim
ihkkim@korea.ac.kr

✉ Kwideok Park
kpark@kist.re.kr

[1] Center for Biomaterials, Korea Institute of Science and Technology (KIST), Seoul 02792, Republic of Korea

[2] Department of Biotechnology, Korea University, Seoul 02841, Republic of Korea

[3] Department of Biochemistry and Molecular Biology, College of Medicine, Asan Medical Center, University of Ulsan, Seoul 05505, Republic of Korea

[4] Department of Pulmonary and Critical Care Medicine, Asan Medical Center, University of Ulsan College of Medicine, Seoul 05505, Republic of Korea

[5] Division of Bio-Medical Science and Technology, KIST School, Korea University of Science and Technology (UST), Seoul 02792, Republic of Korea

Introduction

Human mesenchymal stem cells (MSCs) have been a very promising resource for cell therapy, tissue engineering and regenerative medicine due to their capability of self-renewal and multi-lineage differentiation (Pittenger et al. 1990). Numerous reports have shown therapeutic potential of MSCs via in vitro study or in vivo animal models (Barry and Murphy 2004; Ko et al. 2017; Toh et al. 2012). In addition, many cases of clinical trials via direct MSCs injection are also underway worldwide. A major issue in clinical application of MSCs is to obtain a large quantity of MSCs without compromising intrinsic properties of MSCs throughout ex vivo expansion. Currently, MSCs expansion is mostly achieved via the conventional platform and protocol: tissue culture plastic (TCP) and 10% fetal bovine serum (FBS). For decades, while this combination has been a gold standard in obtaining millions of cells, scientific and clinical studies suggest a need of new protocol for MSCs expansion. The main reason is closely related to replicative senescence of MSCs during a series of cell passaging on TCP (Wagner et al. 2008; Sethe et al. 2006). It is generally accepted that during MSCs expansion there is little chance of malignant transformations but some concerns about genomic mutations (Wang et al. 2013). In this regard, primary interests should be a novel culture platform instead of TCP that has a biomimetic microenvironment similar to the in vivo one. Typical examples are the use of extracellular matrix (ECM) components, such as collagen, fibronectin and laminin, as a culture substratum.

In fact, ECM has a highly organized structure that provides cells with biochemical and biophysical support. Dynamic interactions between cells and ECM play a crucial role in regulating many cellular behaviors. Among different types of ECM, we investigate cell-derived extracellular matrix (CDM) obtained from in vitro cultured mammalian cells. CDM contains major ECM components such as collagen, fibronectin and laminin and presents a self-assembled fibrillar network (Du et al. 2014). CDM has shown very positive effects on hMSCs differentiation and tissue regeneration. Specifically human lung fibroblast-derived ECM could not only improve osteogenic and chondrogenic differentiation of MSCs but also show a much advanced healing effect via a mouse calvarial and rabbit knee articular cartilage defect model (Kim et al. 2015, 2016). Using MSCs-derived ECM, He et al. showed that chondrogenic potential of adipose stem cells (ASCs) expanded on ECM derived from either ASCs or synovium-derived stem cells was much more desirable than those from plastic-grown ones (He and Pei 2013). In addition, Antebi et al. exhibited that stromal cell-derived ECM, formed within a collagen/hydroxyapatite scaffold, promoted MSC proliferation and preserved their differentiation capacity better than MSCs cultured in regular Col/HA scaffolds (Antebi et al. 2015).

Here, we propose human lung fibroblast-derived ECM (hFDM) as a cell expansion platform of human MSCs. Particular interest is the expansion capability of umbilical cord blood-derived mesenchymal stem cells (UCB-MSCs) on hFDM while examining the characteristics of MSCs as compared to TCP and fibronectin (FN)-coated substrate. Recently, decellularized ECM obtained from primary MSCs has emerged as a promising substratum for MSCs expansion (Shakouri-Motlagh et al. 2017; Ng et al. 2014), because it is believed that cells on such ECM may retain their unique characteristics for prolonged times during ex vivo culture (Lai et al. 2010). We assume that because hFDM reserves a natural assembly of ECM components, cell-hFDM interactions should be biomimetic in preserving the intrinsic properties of MSCs. UCB-MSCs are multi-potent progenitors with the potential to differentiate into multiple lineages of the mesoderm, ectoderm and endoderm (Lee et al. 2004; Malgieri et al. 2010). UCB-MSCs are one of the popular cell sources for stem cell therapy and they are more primitive and proliferative than the MSCs obtained from other sources.

In this work, UCB-MSCs adhesion, proliferation, migration and differentiation are directly compared with three different two-dimensional (2D) substrates (TCP and FN-coated TCP, hFDM). Those expanded cells are relocated and cultivated in a 3D polymer mesh scaffold and then examined for osteogenesis, stemness- and engraftment-related markers expression, respectively. In addition, we also investigated a therapeutic effect of MSCs pre-conditioned from different culture substrates via MSCs injection into the animal model of emphysema. Emphysema is a chronic obstructive pulmonary disease that is the main pathological processes of airflow obstruction (Rabe et al. 2007). Patients with emphysema have the damaged lung function for gas exchange and thus suffer from shortness of breath due to over-inflation of the alveoli. This work addresses notable differences of UCB-MSCs behaviors on hFDM as compared to TCP and suggests the possibility of an alternate ex vivo MSCs expansion platform. The overall scheme of this study is illustrated in Fig. 1.

Materials and methods

Preparation of human fibroblast-derived extracellular matrix

Human lung fibroblasts (WI-38, passage 18 to 21; ATCC) were seeded on either 12-well or 6-well plates at a density of 1.25×10^4 cells/cm^2. They were cultivated in Dulbecco's Modified Eagle's medium (DMEM) (Gibco) supplemented with 10% FBS and 100 U/ml penicillin and 100 μg/ml streptomycin (Invitrogen). The medium was changed every other day. Once the cells were fully confluent and the growth medium was then removed, decellularization solution (0.2%

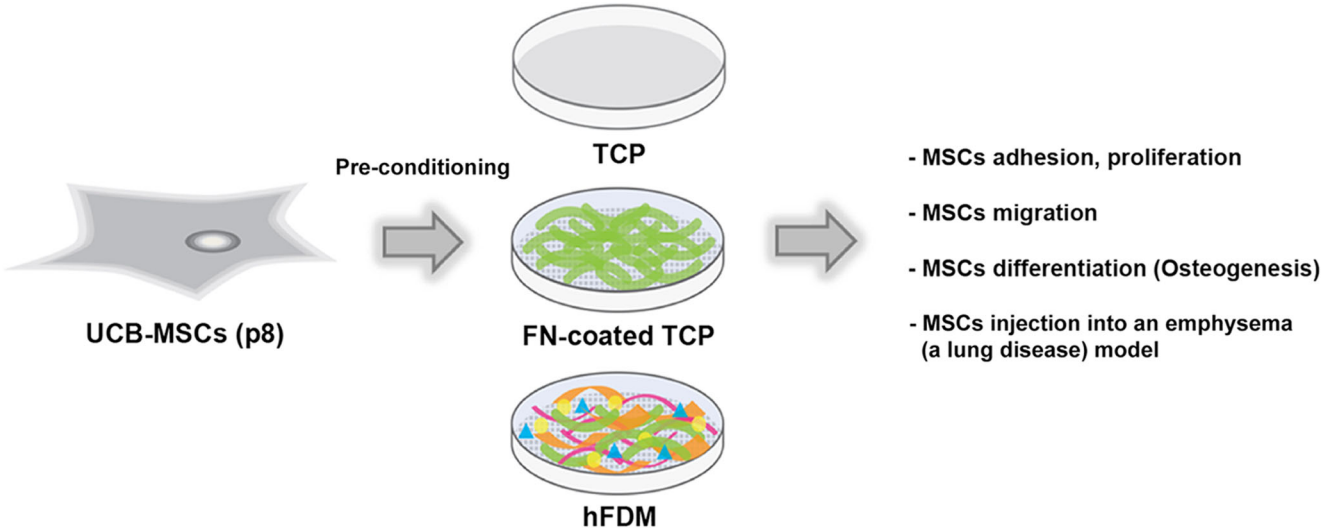

Fig. 1 Schematic illustration of the current study. Based on three different cell expansion platforms (TCP, fibronectin (FN)-coated TCP and hFDM), umbilical cord blood-derived MSCs (UCB-MSCs) adhesion, proliferation, migration and differentiation were investigated. In addition, pre-conditioned MSCs on 2D substrates were detached and transferred to 3D polymer mesh scaffolds and examined for their cellular behaviors, such as proliferation, migration and differentiation. Finally, those UCB-MSCs were subject to direct injection via an emphysema (a lung disease) animal model

Triton X-100 and 10 mM NH_4OH) was added and aspirated in a few minutes. To eliminate the remaining DNA and RNA, 50 U/ml DNase I and 2.5 μl/ml RNase A were subsequently treated for 1 h at 37 °C. After then, the decellularized ECM (hFDM) was washed thoroughly with phosphate-buffered saline (PBS) three times and stored at 4 °C for no longer than 2 weeks.

Umbilical cord blood-derived mesenchymal stem cells culture

For this study, UCB-MSCs were kindly provided from MEDIPOST (Seoul, Korea). UCB-MSCs (P8) were cultured in Minimum Essential Medium Eagle Alpha (α-MEM) (Gibco) supplemented with 10% FBS, 100 U/ml penicillin and 100 μg/ml streptomycin. Cell seeding density was $2.5 \times 10^3/cm^2$ except for the colony-forming unit assay. The medium was changed every other day and UCB-MSCs were allowed to grow until 70 to 80% confluency. For gelatin or FN-coated glass substrates, 18 mm glass coverslips were sterilized in 70% ethanol solution, then put in 12-well plates and coated with 0.5% gelatin or 50 μg/ml human fibronectin (BD Biosciences). They were incubated at 37 °C for 1 h and the remaining protein solutions were aspirated. Those substrates were washed with PBS several times and dried before the use.

Flow cytometry and colony-forming unit-fibroblast assay

UCB-MSCs were cultured on TCP, FN-coated plate and hFDM (100 mm diameter), respectively, before cells reached 70 to 80% confluency. These cells were then harvested from each substrate, washed once with PBS and filtered through a 100 μm cell strainer (BD Falcon) to remove cellular debris. Cells were rinsed again with stain buffer (2% FBS and 0.1% NaN_3, pH 7.1~7.4) and re-suspended to the concentration of 1×10^7 cells/ml. One hundred microliters aliquot out of the cell suspension was taken and transferred to 1.5 ml microcentrifuge tubes for staining procedure. They were incubated with the fluorochrome-conjugated antibodies on ice in the dark for 30 min: phycoerythrin (PE)-conjugated mouse anti-human CD34, allophycocyanin (APC)-conjugated mouse anti-human CD44, fluorescein isothiocyanate (FITC)-conjugated mouse anti-human CD73 and PE conjugated mouse anti-human CD90. All the antibodies were purchased from BD Pharmingen (San Jose, CA, USA). Cells were then washed twice with stain buffer and re-suspended with 500 μl buffer solutions. CD44, CD73 and CD90 are chosen as positive markers of MSCs, whereas CD34 serves as a negative marker. Such markers expression on the cell surface was analyzed using Guava Easycyte (Millipore, Cambridge, MD, USA). For data analysis of cell surface markers, single cell population was gated and Incyte software was used. Meanwhile for colony-forming unit-fibroblast (CFU-F) assay (Moriscot et al. 2015; Li et al. 2013), UCB-MSCs (P8) were plated at a density of 2.5×10^3 cells/cm^2 and cultivated on TCP, FN-coated TCP, and hFDM until 70–80% confluency. Those cells were transferred separately on normal six-well plates at the density of 100 cells/well and subject to colony formation for 10 days. These colonies were stained with 0.5% crystal violet and counted manually. The sample number was triplicate for each group.

Characterization of hFDM

Decellularized hFDM morphology was extracted using a phase contrast microscope. For scanning electron microscope (SEM; Phenom G2 Pro Desktop) observation, hFDM prepared on thermanox (Thermo Scientific; Waltham, MA, USA) was fixed in 3.7% paraformaldehyde for more than 1 h and washed with distilled water (DW), then dehydrated in a series of ethanol concentrations (50 to 100%). They were placed on the aluminum holder, coated with platinum for 45 s and photographed for hFDM surface morphology. For immunofluorescence staining of ECM components, hFDM prepared on glass coverslips was fixed in 3.7% paraformaldehyde and washed with PBS more than three times. The samples were treated with 0.2% Triton X-100 solution for 30 min and then blocked with 3% bovine serum albumin (BSA). Primary antibodies against human fibronectin and collagen type 1 (Santa Cruz) were prepared in 1% BSA solution, diluted in 1: 200 and were treated overnight at 4 °C. As the secondary antibodies diluted in 1: 500, Alexa fluoro-488 was used for fibronectin whereas rhodamine (Invitrogen) was used for collagen type 1. The identity and distribution of these ECM proteins was confirmed via a confocal microscope (LSM700; Carl Zeiss).

Early cell morphology of UCB-MSCs

UCB-MSCs (P8) were plated on gelatin-coated glass coverslips, FN-coated ones and hFDM prepared on glass coverslips. After 6 and 24 h, cells were fixed with 3.7% paraformaldehyde and incubated with primary antibody that is mouse monoclonal antibody against human vinculin (sc-73614, Santa Cruz) overnight at 4 °C. Alexa Fluor 488 goat anti-mouse IgG antibody (A11001, Life technology) was employed as a secondary antibody. During secondary antibody staining, rhodamine phalloidin (R415, Life technology) was added for F-actin staining. Eventually the samples were mounted with a mounting medium including 4′,6-diamidino-2-phenylindole (DAPI) (Vector). Immunofluorescence images were acquired using a confocal microscope (Carl Zeiss). Using multiple fluorescent images ($n = 20$, each group), both cell area and cell circularity were quantified and averaged, respectively, via Image J.

Cell proliferation and migration assay

UCB-MSCs (P8) were seeded on TCP, FN-coated TCP and hFDM (six-well plate size) at a density of $2.5 \times 10^3/cm^2$ in 2 ml culture medium. On the 3rd and 5th day of culture, the cell numbers of each group were determined by CCK-8 assay (Dojindo) according to the manufacturer's protocol. The absorbance of each sample was measured at 450 nm wavelength using Multiskan spectrum (Thermo Electron Corporation; Waltham, MA, USA). Cell expansion under 10 and 2% FBS condition was also examined following the same procedure. In addition, different UCB-MSCs passages (P6 and P11) were also tested for cell proliferation on the same substrates in 10% serum condition. Based on the cell numbers as determined by CCK-8 assay, population doubling time (PDT) was calculated via an equation, $PDT = \text{culture time} / (\log_2 (\Delta N/N_0 + 1))$, where ΔN is the difference between cell numbers at two time points and N_0 is the cell number at the starting point (Korzyńska and Zychowicz 2008). Meanwhile for the cell migration test, UCB-MSCs were seeded and cultivated until full confluency on TCP (35 mm diameter), FN-coated TCP and hFDM. Artificial wounds were then made via 1000 μl micropipette tip and cells were allowed to migrate across the scratched area for 24 h in serum-free media with 50 ng/ml stromal cell-derived factor (SDF)-1 treatment. Cell migration with time was monitored via a live cell image microscope (Carl Zeiss, Germany) and those images were taken at 12 and 24 h, respectively. Upon the treatment of 10 and 50 ng/ml SDF-1, CXC chemokines platelet factor-4 (CXCR4) expression on different substrates or under lower FBS concentration was also determined, using quantitative real-time polymerase chain reaction (qPCR).

Quantitative real-time polymerase chain reaction

For the analysis of specific gene expression, total mRNA of UCB-MSCs grown on different substrates or cultivated in a three-dimensional (3D) mesh scaffold was extracted at specific time points, using TRIZOL reagent in accordance with the manufacturer's instruction. The quantity and quality of RNA samples ($n = 3$, each group) were examined by NanoDrop ND-1000 spectrophotometer (Thermo Fisher Scientific, Wilmington, DE). One microgram mRNA per sample was used for cDNA synthesis via Maxime RT PreMix Kit (INTRON) at 37 °C for 15 min and RTase inactivation at 85 °C for 5 s. The cDNA product, each reverse and forward primer, SYBR Green real-time PCR mix (RR420A; Takara) and ROX reference dye were mixed in PCR reaction tubes (Applied Biosystems) to a total volume of 20 μl, where the reaction conditions are initial denaturation and DNA polymerase activation at 95 °C for 5 min, followed by 40 cycles of denaturation at 95 °C for 5 s and annealing/extension at 60 °C for 34 s. The reaction reagents were blended thoroughly, centrifuged shortly and then loaded in the qPCR instrument (7500 Real-Time PCR System; Applied Biosystems). The data from qPCR were analyzed via the delta delta Ct method. Target genes and their primer sequences are summarized in the Supplementary Information (Table 1).

Table 1 List of target genes and their primers sequence used in this study

Primers	Sequence	Product size
BMI1	F: TTCTTTGACCAGAACAGATTGG R: GCATCACAGTCATTGCTGCT	112 bp
EZH2	F: GGACCACAGTGTTACCAGCAT R: GTGGGGTCTTTATCCGCTCAG	79 bp
NANOG	F: TGGCTGCCGTCTCTGGCTATAGAT R: AAGCCTCCCAATCCCAAACAATAC	143 bp
OCT 4	F: AGCAAAACCCGGAGGAGT R: CCACATCGGCCTGTGTATAT	114 bp
CXCR4	F: CTCCAAGCTGTCACACTCCA R: GTCGATGCTGATCCCAATGT	118 bp
SDF-1	F: TGCCAGAGCCAACGTCAAG R: CAGCCCGGCTACAATCTCAA	73 bp
Col1	F: CTGGATGCCATCAAAGTCTTC R: AATCCATCGGTCATGCTCTC	152 bp
RUNX2	F: TGCACTGGGTCATGTGTTTG R: TGGCTGCATTGAAAAGACTG	154 bp
Osteocalcin	F: GGCAGCGAGGTAGTGAAGAG R: AGCAGAGCGACACCCTAGAC	194 bp
Osteopontin	F: TGAAACGAGTCAGCTGGATG R: TGTGAAAATTCATGGCTGTGG	165 bp

Osteogenic differentiation of UCB-MSCs in vitro

UCB-MSCs (P8) were subject to osteogenic differentiation on TCP, FN-coated plate and hFDM for 2 weeks. After the cells reached 70–80% confluency, growth medium was removed and an osteogenic medium (0.1 μM dexamethasone, 10 mM β-glycerophosphate, 50 μg/ml L-ascorbic-2-phosphate and 50 ng/ml bone morphogenetic protein-2) was added. Fresh osteogenic medium was replenished every third day. After 2 weeks of osteogenic induction, cells were fixed using 3.7% paraformaldehyde, washed three times with DW thoroughly and stained via *von Kossa* and Alizarin red staining, respectively. Once dehydrated and completely dried, each sample ($n = 3$, each group) was observed under bright field, in which the images of interest were taken and analyzed using Image J. With color threshold function and the same value on "Brightness," the positively stained area was selected ($n = 15$, each group) and averaged. The stained areas were normalized to the whole area of the images and appeared as a percentage in the graph. In addition, alkaline phosphatase (ALP) activity ($n = 3$ per group) was also measured using LabAssay ALP kit (Wako Pure Chemicals, Osaka, Japan) following the previous protocols (Du et al. 2014). In a separate study, different cell passages (P6 and P11) were also examined for osteogenic differentiation on the same substrates as assessed via *von Kossa* staining and gene expression of osteogenic markers, respectively.

UCB-MSCs behavior in 3D polymer mesh scaffold

In addition to 2D culture on varying substrates, a further comparative evaluation of UCB-MSCs responses was carried out via a 3D environment. Poly (lactic-co-glycolic acid) (PLGA)-based mesh scaffolds were fabricated as mentioned previously (9), cut in $0.5 \times 0.5 \times 0.5$ cm^3 dimension and dipped in 100% ethanol for 5 min, then completely dried for more than 2 h under UV light for sterilization. They were then treated with 50 μg/ml of human fibronectin (BD Biosciences) on the surface of the mesh scaffold for 24 h at 37 °C, washed with DW and cryodessicated. Once UCB-MSCs (P8) were expanded on TCP, FN-coated TCP and hFDM, those confluent cells were harvested and transferred into mesh scaffolds at a density of 1×10^4 cells. After 2 h post-seeding, 1 ml of additional growth medium was added and cells/mesh constructs were cultivated for specific time points. For cell proliferation, the number of cells was assessed at 0 and 5 days, respectively, via CCK-8 assay. On the 8th day of culture, 50 ng/ml SDF-1 was added into the constructs and after 24 h, gene expression of CXCR4 was determined following the same method as mentioned earlier. Meanwhile, UCB-MSCs (P8) grown on TCP and hFDM in 2 or 10% serum condition were collected and reseeded in the mesh scaffolds. They were cultivated for 10 days and gene expressions of stemness-related markers (NANOG, EZH2, BMI-1, OCT4) and engraftment-related ones (MMP2, MMP9, CXCR4, SDF-1) were determined via qPCR. In addition, osteogenic induction of mesh scaffold-seeded UCB-MSCs was also conducted for 2 weeks following the same protocol previously mentioned. Using the isolated total RNA samples from mesh scaffolds, we examined osteogenic markers expression (runx2, collagen type 1, osteocalcin, osteopontin) via qPCR.

Cell transplantation into elastase-induced lung disease (emphysema) model

An animal model with a lung disease (emphysema) was prepared as mentioned previously (Hong et al. 2016) and subject to UCB-MSCs injection as cell therapy. The current animal experiment follows the guidelines of the Institutional Animal Care and Use Committee, Asan Medical Center (Seoul, Korea). MSCs were expanded on TCP and hFDM in 10 and 2% serum condition, respectively. There are four experimental groups: G1 (TCP/10% serum), G2 (TCP/2% serum), G3 (hFDM/10% serum) and G4 (hFDM/2% serum), along with a normal group and a no MSCs treatment one. C57BL/6 mice were anesthetized intraperitoneally (i.p.) with 16 ml of Zoletil 50 (Virbac Laboratories, Carros, France) and 4 ml of Rompun (Bayer Korea, Ansan, Korea). To prepare an elastase-induced lung disease model, mice were intratracheally administered using porcine pancreatic elastase (0.4 U, 8 U/ml; Sigma-Aldrich, St. Louis, MO) at day 0. After 7 days, mice ($n = 5$,

each group) were intrapleurally injected with UCB-MSCs (1×10^5: P8) using a syringe of 26-gauge needle. As the animals were sacrificed at 1 week post-treatment, histological analysis of the lung tissues was carried out using the established protocol. Briefly, the perfused lungs were inflated with 0.5% low-melting agarose, fixed with 4% formalin and embedded in paraffin. Lung tissue sections with a thickness of 6 μm were subject to hematoxylin and eosin staining. A mean linear intercept (MLI), an index that shows the degree of lung alveolar damage, was determined from the microscopic images ($n = 5$, each group); less MLI means a positive sign of improvement with an increased surface area of alveolar.

Statistical analysis

Statistical analysis of the obtained data was performed using commercial software (GraphPad Prism 5; GraphPad Software Inc.) via one-way analysis of variance and Mann Whitney post hoc test. Each sample was triplicate per group. All of the data represent the mean values and standard deviations. Statistical significance was marked as *($p < 0.05$), **($p < 0.01$), or ***($p < 0.001$).

Results and discussion

Since large in vitro expansion of MSCs is an essential process for stem cell therapy and tissue regeneration, traditional cell culture plastic has been widely utilized for cell expansion. However, stem cells often lose their unique characteristics during a series of passaging that is a necessary step to produce large quantity of cells in vitro. Therefore, maintenance of the intrinsic properties of MSCs during expansion is considered a major issue in stem cell-based research and therapy, along with the safety of those expanded cells. This study harnesses hFDM as a platform of MSCs expansion in vitro. hFDM is a naturally derived ECM, which contains a comprehensive package of well-reserved biochemical and biophysical cues (Cukierman et al. 2001) and thus is a promising alternative to tissue culture plastic.

hFDM is consistent in terms of ECM quality as assessed via immunofluorescence and SEM image: fibronectin, the most important ECM molecule for cell adhesion, is well distributed over the entire area and the fibrillar structure of hFDM is also witnessed (data not shown). Moreover, quality control of CDM may be better with cell lines, in which cell-to-cell variations are minimal than primary cell sources. We also believe that human lung fibroblast is a cost-effective cell source. It is notable that though CDM is an excellent material for regenerative purpose, a major hurdle is the scalability of CDM for mass production. There are some reports that utilize immortalized cell lines as an alternative cell source (Kusuma et al. 2017, 2018). Nonetheless, there is still no consensus about which CDM is better for a regenerative purpose. The exact reason about why hFDM shows better performance over the counterparts is hard to pinpoint, because hFDM is a complex system that involves many individual constituents.

After the decellularization process is completed, hFDM shows a unique surface morphology when observed via an optical microscope and SEM (Fig. 2a, b). Phase contrast image exhibits a fibrous structure of hFDM and SEM shows fine fibrillar textures clearer over the entire matrix. In addition, immunofluorescence staining unveils the presence of ECM macromolecules: fibronectin (Fig. 2c) and collagen type I (Fig. 2d) in the hFDM. These results assure the quality of hFDM as a multi-component, fibrous ECM analog. With hFDM on hand, once UCB-MSCs were seeded and expanded on three different substrates (TCP, FN-coated TCP and hFDM) until 70–80% confluency, basic characteristics of MSCs were evaluated via flow cytometry and CFU-F assay. The MSCs populations show that regardless of substrate types, cell surface markers were positive with CD44 (> 85%), CD73 (> 98%) and CD 90 (> 99%) but negative with CD34 (a hematopoietic marker) (< 0.1%) (Fig. 3a–d, a′–d′, a″–d″). In addition, when those MSCs grown on each substratum were transferred to TCP and cultivated for 10 days, they could form some colonies (Fig. 3e–e″), suggesting a self-renewal property of UCB-MSCs. Based on the counts of each colony, there was a statistically significant difference between those on FN/TCP and hFDM/TCP (Fig. 3f).

Early cell morphology was also examined via immunofluorescence of F-actin cytoskeleton, along with a focal adhesion molecule (vinculin) staining. After 24 h post-seeding, cells have a rounded morphology on gelatin (Gn) but a more widely spread shape on hFDM than the other substrates (Fig. 4a–c). The expression of focal adhesion molecules was more up-regulated on hFDM. Quantitatively analyzed, the results showed significantly larger cell areas on FN and hFDM (Fig. 4d) and presented cell circularity much lower on hFDM (Fig. 4e). The difference of such parameters was statistically significant between hFDM and TCP or the FN-coated plate. Comparatively, MSCs morphology is notable, especially on hFDM and can be partly explained by the more complex nature of cell-substrate interactions: unique surface texture and rich cell-binding motifs that are significantly different from those on the traditional substrates may influence cell adhesion pattern.

Cell proliferation efficiency is technically an important issue in preparing stem cell therapy. To evaluate the growth of UCB-MSCs, cells were cultivated on three different substrates and collected on 3 and 7 days, respectively, for CCK-8 assay. From the phase contrast images, cells appeared much more populated on hFDM compared to the others (Fig. 5a–c). As a measure of cell proliferation, PDT presented shorter PDT with the cells grown on hFDM, both in 2 and 10% serum conditions (Fig. 5d). It seems natural that PDT climbs when

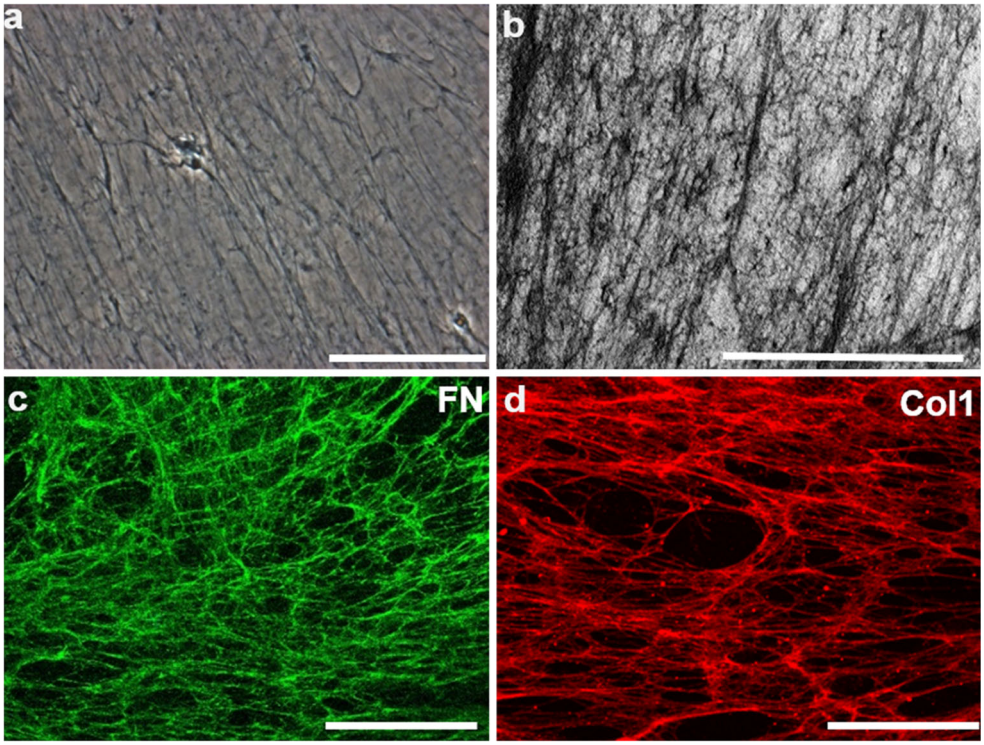

Fig. 2 Characterization of hFDM. Human fibroblast-derived extracellular matrix (hFDM) is obtained from decellularized ECM derived from in vitro cultured lung fibroblasts. Some important characteristics of hFDM were investigated via **a** phase contrast microscopic image of hFDM (scale bar = 100 μm); **b** SEM image (scale bar = 130 μm), immunofluorescence of (**c**) fibronectin and (**d**) collagen type 1 (scale bar = 200 μm)

cells were cultivated in 2% FBS. Upon the shift from 10 to 2% serum, the difference of PDT was much smaller with hFDM than that of TCP or FN substrate. Additionally, as the cell numbers are quantitatively determined, in 10% FBS condition the cell number on hFDM was about 1.8-fold higher than that on TCP at 7 days (Fig. 5e). The difference was even

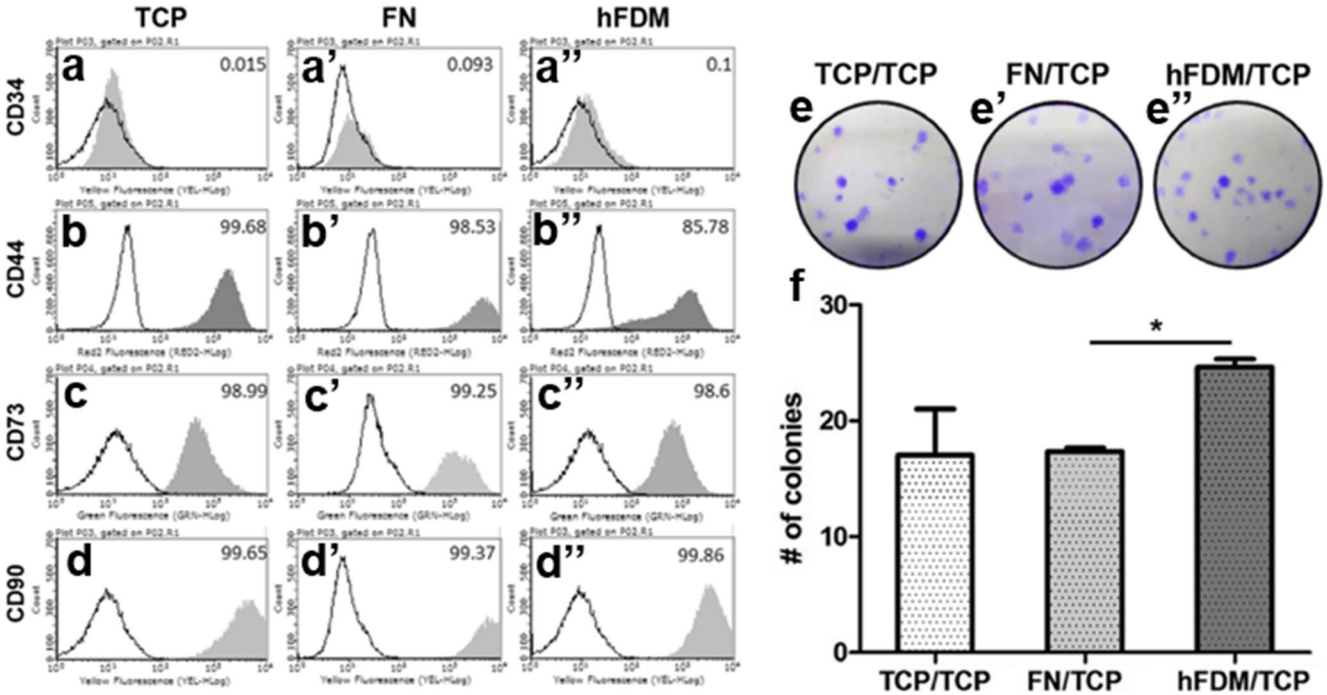

Fig. 3 Characterization of UCB-MSCs. **a**–**d**, **a′**–**d′**, **a″**–**d″** Flow cytometry and **e**–**e″** colony forming unit-fibroblast (CFU-F) assay and **f** quantitative analysis of colony number. Once UCB-MSCs were cultivated and expanded on TCP, FN-coated TCP and hFDM, they were then analyzed via cell surface markers, such as CD34, CD44, CD73 and CD90. In addition, MSCs on three different substrates were harvested, seeded on six-well plates and incubated for 10 days, then subject to crystal violet staining. The number of colonies was manually counted. Statistical significance (*$p < 0.05$)

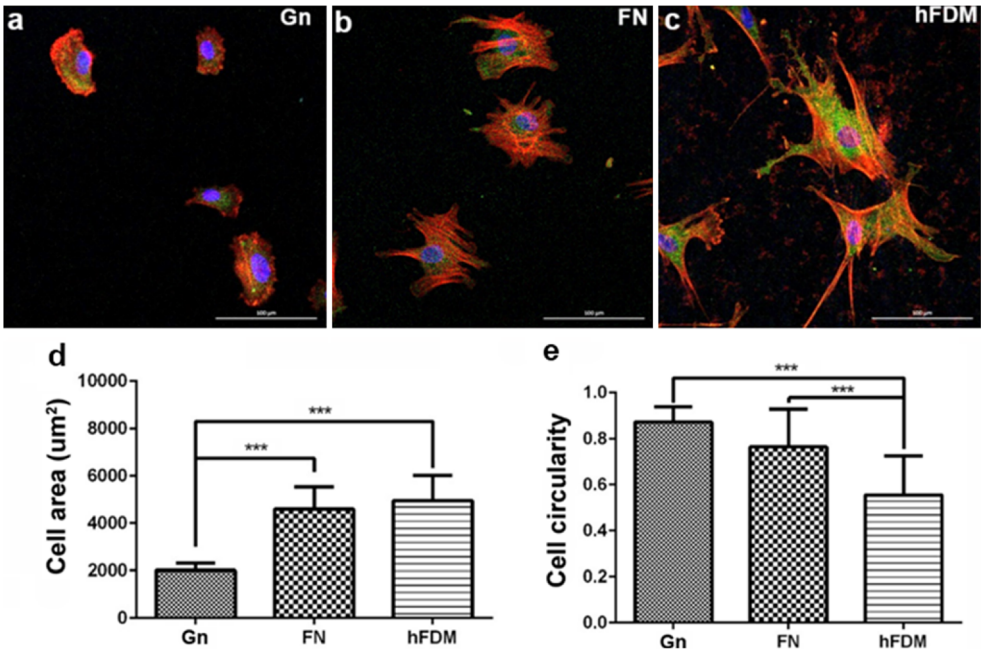

Fig. 4 Early cell morphology (24 h) of UCB-MSCs and focal adhesion. **a**–**c** Representative immunofluorescence images of UCB-MSCs attached on gelatin (Gn)-coated glass coverslip, FN-coated one and hFDM. Quantitative analysis of **d** cell area and **e** cell circularity. Vinculin (green), F-actin (red) and DAPI (blue). Scale bar = 100 μm. Statistical significance (***$p < 0.001$)

greater when compared with the number on the FN-coated plate. This trend is replicated in 2% serum condition: the cell populations on hFDM were significantly larger at 7 days than those on the other substrates. It is notable that the cell numbers on hFDM in 2% serum were nearly the same at 7 days as those on TCP under 10% serum (Fig. 5e, f). Due to the fact that cells are very slow in their growth activity in the lower serum condition, it is very interesting that a specific substrate microenvironment enhances the cell proliferation rate significantly. In addition, when UCB-MSCs proliferation using different cell passages (P6 and P11) was examined under the 10% serum condition, the results were reproducible when compared with those of P8; the difference was notable with hFDM at 7 days and statistically significant over TCP and FN-coated TCP (Fig. S1a, b).

Current results suggest that hFDM could provide MSCs with some biochemical and/or biophysical signaling cues that are unknown at this time but regulate their proliferation potential in vitro. Much research has reported on the proliferation rate of human adult stem cells on diverse ECM-based 2D substrates in 10% FBS condition. For example, Matrigel improved cell expansion (1.6-fold) of human MSCs (Qian and Saltzman 2004) and decellularized ECM from human BMSCs could enhance cell proliferation (2- to 4-fold) of human BMSCs (Lin et al. 2012). In addition, the combination of collagen I/collagen IV with laminin and fibronectin showed an increased cell expansion of human hematopoietic progenitors (Celebi et al. 2011). Compared to previous reports, the current result of hFDM is comparable in terms of MSCs proliferation efficiency

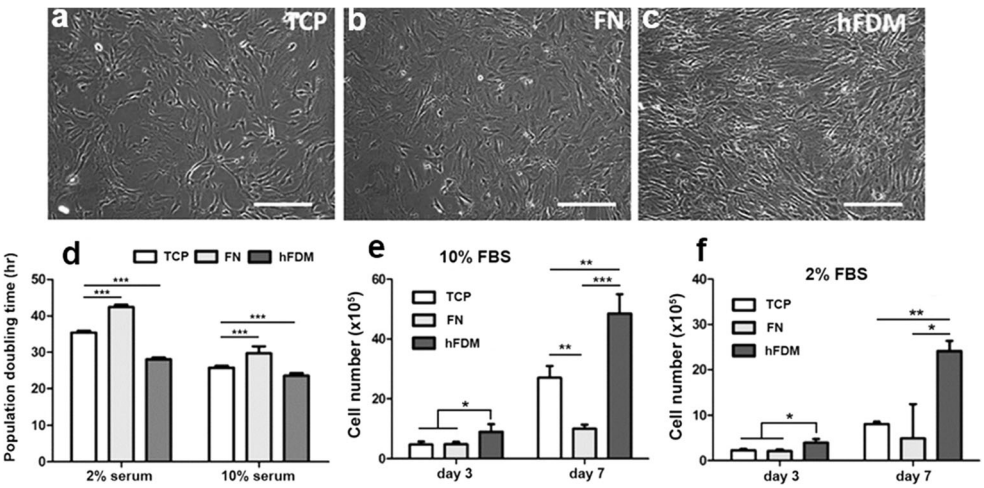

Fig. 5 Examination of MSCs proliferation on three different substrates. **a**–**c** Phase contrast images of UCB-MSCs on the 5th day of culture on TCP, FN-coated TCP and hFDM. Once the cell number of each group was determined using CCK-8 assay, **d** population doubling time (PDT) was determined. Cell proliferation was examined via UCB-MSCs cultured for 3 and 7 days in **e** 10% and **f** 2% serum condition, respectively. Scale bar = 500 μm. Statistical significance (*$p < 0.05$, **$p < 0.01$, ***$p < 0.001$)

and is the first report that directly compares MSCs proliferation between 10 and 2% serum condition.

Meanwhile, cell migration of MSCs is critical in improving the cell homing effect once MSCs were transplanted to target sites in vivo for therapeutic purpose. MSCs are often stimulated via SDF-1, a chemokine signaling molecule, also known as C-X-C motif chemokine 12 (CXCL12) that is often released from wounded areas. SDF-1 binds to its transmembrane receptor CXCR4. Some studies have suggested SDF-1 as a crucial factor in prompting the survival and migration of circulating tissue-specific progenitor cells (Kucia et al. 2004). In this study, cell migration of UCB-MSCs was investigated using a simple scratch model in a serum-free condition. Phase contrast images display a scratched, wound area at 0 h and wound closure via migrating cells after 24 h (Fig. 6a–c, a′–c′). When the number of cells covering the wound area was quantitatively determined, the cells on the hFDM exhibited substantially more migrated cells than those grown on TCP (Fig. 6d). It seems that our scratch model is too simple to precisely evaluate cell migration activity on different substrates. In fact, many parameters affect cell migration: for example, ligand type, ligand density and ligand distribution on a specific substrate. It was not affordable however for us to consider those factors in this study, due mainly to totally different starting materials (TCP, FN and hFDM). Our recent data using soluble hFDM demonstrate a chemoattractant effect of hFDM in transwell that shows much better cell migration of dermal fibroblasts and human umbilical vein endothelial cells (data not shown). As a part of the mechanistic study, our previous work reported that hFDM carries abundant biochemical cues, such as angiogenesis-related cytokines and growth factors (VEGF, bFGF, SDF-1) (Du et al. 2017).

We also examined the responsiveness of UCB-MSCs to SDF-1 via the use of 10 and 50 ng/ml SDF-1, respectively, for the cells on TCP, FN, or hFDM. After 24 h post-treatment, gene expression of CXCR-4 showed a significantly higher level with hFDM administered with 10 ng/ml SDF-1 over the other two substrates (Fig. 6e). When 50 ng/ml of SDF-1 was administered, the CXCR-4 expression was dose-dependent: especially cells on TCP and FN exhibited a significant up-regulation of target genes compared to that of 10 ng/ml SDF-1. However, the expression level of CXCR-4 was rather unchanged with the hFDM, despite the use of a higher dose of SDF-1 (50 ng/ml). In addition, further study investigated the CXCR-4 expression of UCB-MSCs under different serum conditions (2 and 10%) (Fig. 6f). When the cells were seeded on hFDM, added with 10 ng/ml SDF-1 and cultivated for 7 days, the gene expression level of CXCR-4 was highest with those cultivated on hFDM/2% serum. The difference was statistically significant over the TCP/10% or hFDM/10% group. Taken together, the notably different cell responsiveness (CXCR4 expression) after the SDF-1 treatment suggests that it can be highly dependent of the unique characteristics of culture substrates.

To investigate the differentiation of UCB-MSCs grown on different substrates, UCB-MSCs were subject to osteogenic induction for 2 weeks and analyzed. When mineralization was examined via *von Kossa* staining, it was clear that cells cultivated on hFDM exhibited much better mineralization

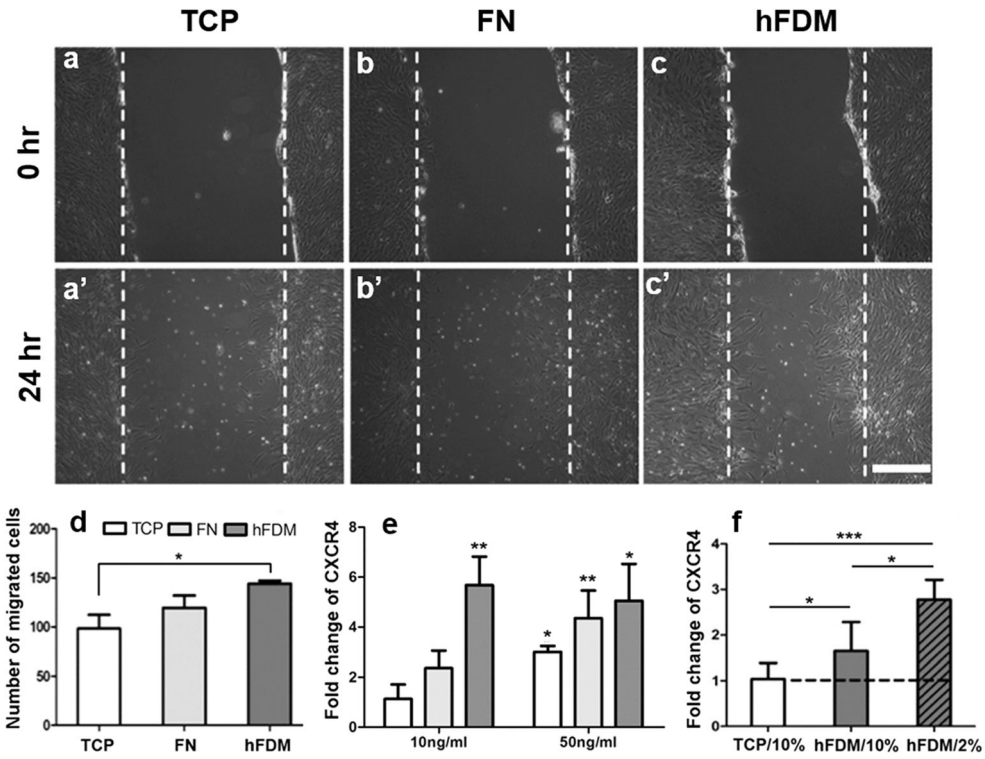

Fig. 6 MSCs migration and CXCR4 expression. Migration capability of UCB-MSCs on three different substrates was examined using scratch assay and CXCR4 gene expression via qPCR. **a**–**c**, **a′**–**c′** Representative optical images of MSCs before and after migration for 24 h; **d** count of the cells number occupied in the scratched area; **e** CXCR4 expression level with 10 and 50 ng/ml SDF-1 treatment, respectively (TCP-10 ng/ml based statistical comparison); **f** the CXCR4 expressions in 2 and 10% serum condition, respectively. Scale bar = 500 μm. Statistical significance (*$p < 0.05$, **$p < 0.01$, ***$p < 0.001$)

(Fig. 7a–a″). Quantitatively assessed, the difference of the positively stained area was statistically significant between hFDM and TCP or FN substrate (Fig. 7b). The same trend was also observed via Alizarin red staining (Fig. 7c–c″, d). Measurement of ALP activity showed a moderate improvement with hFDM (Fig. 7e). In addition, osteogenic markers expression revealed that both type I collagen and osteocalcin were substantially up-regulated with the cells on the hFDM over TCP and FN (Fig. 7f, g). In addition, as the osteogenic differentiation of UCB-MSCs with different cell passages (P6 and P11) was directly compared under the same condition, the results were reproducible with P11 rather than early passage P6 when compared with those of P8 (Fig. S2a–d). The difference was notable with hFDM and statistically significant over the two counterparts. Current results are in good agreement with our early works using bone marrow stromal cells and rat bone marrow MSCs (Bae et al. 2012; Choi et al. 2014). Due to the fact that substrate stiffness is recognized as a key factor in the regulation of MSCs differentiation, it is interesting to note much advanced osteogenesis of MSCs on cell-derived ECM that is extremely softer than TCP. Although the exact reason is unclear at this time, there are many possibilities for other unknown factors that direct MSCs differentiation and therefore they may override the substrate stiffness-related signaling cues.

It is well known that culture environments in 2D or 3D settings affect cellular behaviors in significantly different ways. In this sense, we utilized a polymer mesh scaffold to grow UCB-MSCs that were expanded on TCP and hFDM in 2 or 10% FBS condition, respectively. These 3D mesh scaffolds were successfully fabricated and employed in inducing both osteogenesis and chondrogenesis of hMSCs in vitro and in vivo (Kim et al. 2015, 2016). After cultivated in the mesh scaffolds for 10 days, UCB-MSCs showed more up-regulation of stemness markers (NANOG, EZH2, BMI1) when conditioned on hFDM compared to those on TCP, although some variations were noticed in either 2 or 10% serum condition (Fig. 8a–d). In addition, some of the engraftment-related markers (MMP9, CXCR4) also demonstrated much higher gene expression with MSCs conditioned on hFDM/10% serum (Fig. 8e–h). Further analysis of cell proliferation in the mesh scaffolds from day 0 to 5 showed better proliferation of UCB-MSCs transferred from hFDM than that of FN/Mesh (Fig. S3a). And UCB-MSCs conditioned on hFDM unveiled significantly higher expression of cell migration-related marker (CXCR4) over those conditioned on TCP or FN-coated substrate (Fig. S3b). In case of osteogenesis, only collagen type I was notably expressed in the hFDM/Mesh but the difference

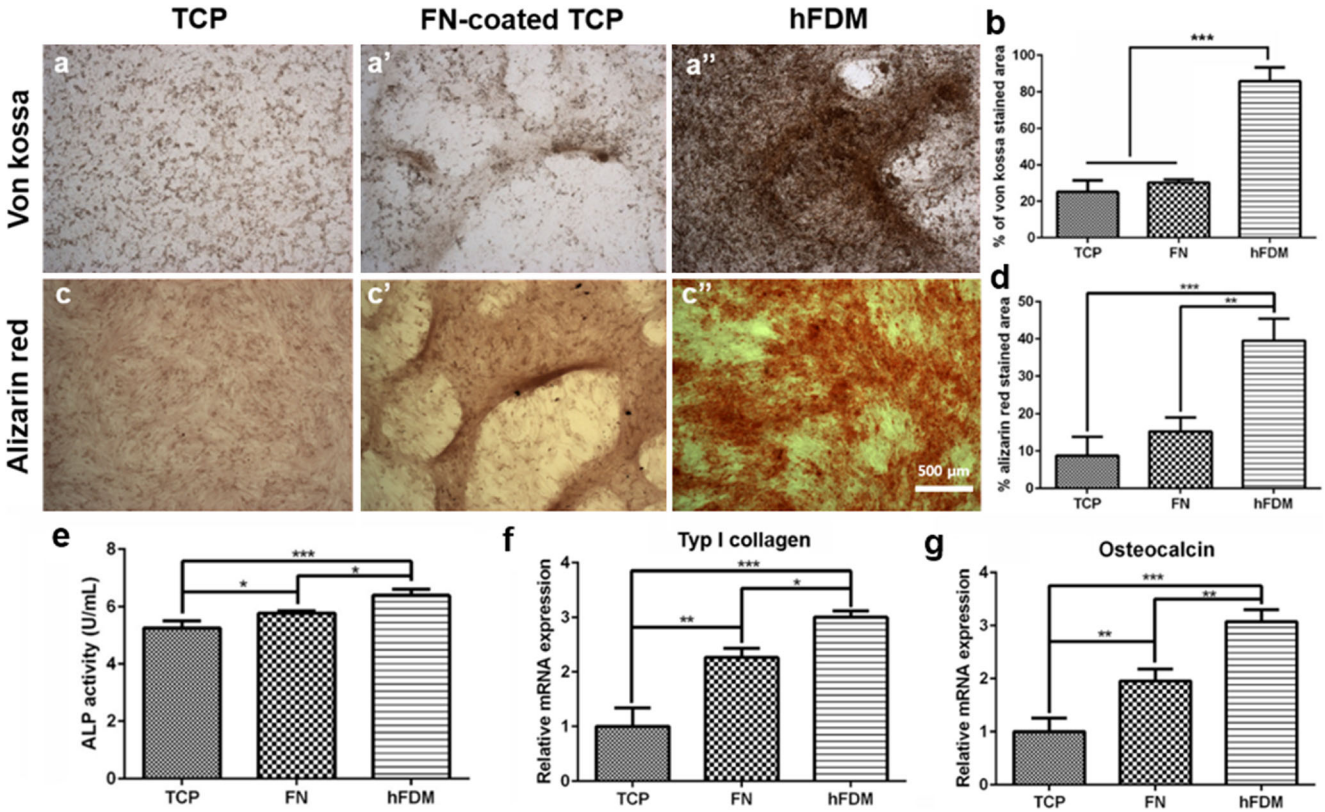

Fig. 7 Osteogenic differentiation of UCB-MSCs in vitro. UCB-MSCs cultured on TCP, FN-coated TCP and hFDM were subject to osteogenic differentiation for 2 weeks. Bright field images of **a**–**a**″ *von Kossa* and **c**–**c**″ Alizarin red staining; **b**, **d** quantitative analysis of a positively stained area using ImageJ. **e** Measurement of alkaline phosphatase (ALP) activity and **f**, **g** gene expression of osteogenic markers (collagen type I and osteocalcin) via qPCR. Scale bar = 500 μm. Statistical significance (*$p < 0.05$, **$p < 0.01$, ***$p < 0.001$)

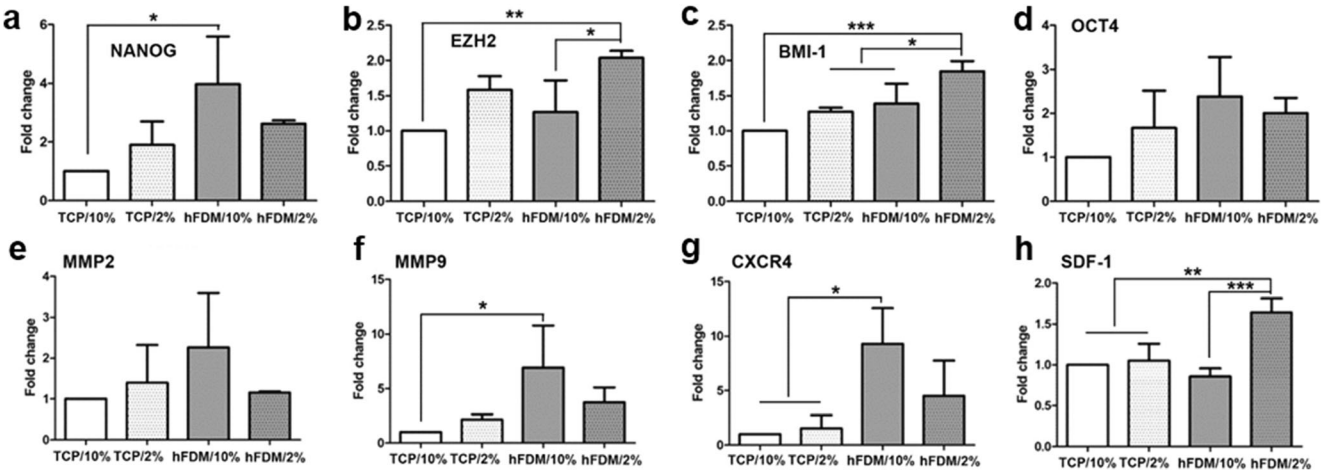

Fig. 8 Gene expression of stemness- and engraftment-related markers in 3D polymer mesh scaffolds. Once UCB-MSCs were expanded on TCP, FN-coated TCP and hFDM, those confluent cells were collected and reseeded into mesh scaffolds, cultivated for 10 days, then analyzed via qPCR. **a**–**d** Gene expression of stemness-related markers (NANOG, EZH2, BMI-1, OCT4) and **e**–**h** engraftment-related ones (MMP2, MMP9, CXCR4, SDF-1). Statistical significance (*$p < 0.05$, **$p < 0.01$, ***$p < 0.001$)

of other markers (Runx2, osteopontin, osteocalcin) expression was insignificant (Fig. S3c).

Based on the in vitro results, it is apparent that UCB-MSCs conditioned on hFDM are more competitive in terms of MSCs proliferation, migration and differentiation than those on TCP. In this sense, particular interest lies in the therapeutic effect of hFDM-conditioned UCB-MSCs to a specific disease model. To verify our hypothesis, we prepared four different groups of UCB-MSCs and administered them into an emphysema (a lung disease) model. Chronic obstructive pulmonary disease (COPD), which is a major cause of mortality worldwide, is a disease state characterized by airflow obstruction that is not fully reversible. Although the pathogenesis of COPD is incompletely understood, emphysema and small-airway disease are the main pathological processes in the development of airflow obstruction. An emphysema model was prepared using elastase and subject to UCB-MSCs injection. Those MSCs were expanded on TCP or hFDM in both 10 and 2% serum conditions. Once four experimental groups were executed with MSCs administration intrapleurally, the results indicated that all of the MSCs-treated groups exhibited an improvement compared to the non-treated one (Ela) as assessed via the MLI values (Fig. 9a–f). MLI is an index that semi-quantitatively determines the alveolar size, where higher MLI is a suggestive of reduced alveolar surface area. The

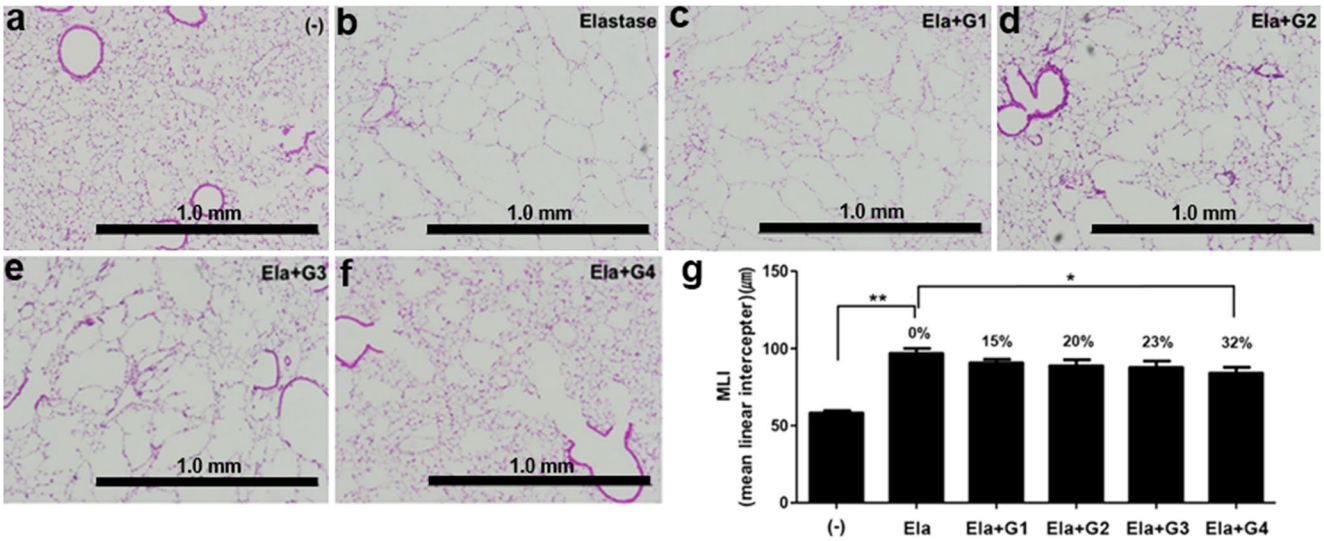

Fig. 9 Therapeutic effect of UCB-MSCs injection via an emphysema (a lung disease) animal model. The emphysema model was prepared using elastase and subject to MSCs injection intrapleurally. Those MSCs were expanded on TCP and hFDM in 10 and 2% serum condition, respectively. Experimental groups are G1 (TCP/10% serum), G2 (TCP/2% serum), G3 (hFDM/10% serum) and G4 (hFDM/2% serum), along with a normal group (−) and no MSCs treatment group (Ela). **a**–**f** Optical images of lung tissues after H&E staining and **g** quantitative analysis of therapeutic index (MLI). Scale bar = 1.0 mm. Statistical significance (*$p < 0.05$, **$p < 0.01$)

histological images show that the normal group has many small and compact alveolar that give a higher surface area and present a much lower MLI, whereas the non-treated group exhibits a large and loose alveolar structure. An early study of Ueno et al. investigated the effect of oral administration of alendronate on elastase-induced pulmonary emphysema in mice and evaluated the therapeutic efficacy using the MLI (Ueno et al. 2015). It is notable however that quantitatively assessed, only the group of UCB-MSCs conditioned on hFDM (2% serum) showed a statistically significant difference of the MLI compared to the no treatment group ($p < 0.05$) (Fig. 9g). A previous study suggested that administration of bone marrow cells (BMCs) or MSCs exhibited the therapeutic capability in improving cigarette smoke-induced emphysema in rats (Huh et al. 2011). In addition, Hong et al. evaluated the therapeutic effects of pioglitazone-pretreated human adipose-derived mesenchymal stem cells (ASCs) on the emphysema models in mice (Hong et al. 2016). They concluded that pioglitazone-pretreated ASCs resulted in a more potent therapeutic effect than non-pretreated ASCs in the recovery of both elastase-induced and smoke-induced emphysema models.

Conclusions

In this study, hFDM demonstrates its feasibility as a MSCs expansion platform compared to TCP and FN-coated substrate. UCB-MSCs exhibited not only highly improved cell proliferation on hFDM under both lower and high serum conditions but also showed better cell migration and differentiation capability in vitro. In addition, when UCB-MSCs were transferred to a 3D polymer mesh scaffold, MSCs conditioned on the hFDM presented highly up-regulated gene expression of stemness- and engraftment-related markers. Moreover, UCB-MSCs injection via an emphysema (a lung disease) animal model demonstrated that MSCs cultivated on hFDM in 2% serum condition resulted in more beneficial therapeutic efficacy than those on TCP. Taken together, current works strongly suggest that hFDM does hold ECM microenvironments suitable for MSCs proliferation, migration and differentiation when they were cultivated in a monolayer. Therefore, hFDM can be a promising alternative to TCP as a cell expansion platform.

Funding information This study was supported by the Korea Health Industry Development Institute (KHIDI) and funded by the Ministry of Health and Welfare (HI16C0133), Republic of Korea.

Compliance with ethical standards

Competing interest The authors declare that they have no competing financial interests.

References

Antebi B, Zhang Z, Wang Y, Lu Z, Chen XD, Ling J (2015) Stromal-cell-derived extracellular matrix promotes the proliferation and retains the osteogenic differentiation capacity of mesenchymal stem cells on three-dimensional scaffolds. Tissue Eng Part C Methods 21:171–181

Bae SE, Bhang SH, Kim BS, Park K (2012) Self-assembled extracellular macromolecular matrices and their different osteogenic potential with preosteoblasts and rat bone marrow mesenchymal stromal cells. Biomacromolecules 13:2811–2820

Barry FP, Murphy JM (2004) Mesenchymal stem cells: clinical applications and biological characterization. Int J Biochem Cell Biol 36: 568–584

Celebi B, Mantovani D, Pineault N (2011) Effects of extracellular matrix proteins on the growth of haematopoietic progenitor cells. Biomed Mater 6:055011

Choi DH, Suhaeri M, Hwang MP, Kim IH, Han DK, Park K (2014) Multi-lineage differentiation of human mesenchymal stromal cells on the biophysical microenvironment of cell-derived matrix. Cell Tissue Res 357:781–792

Cukierman E, Pankov R, Stevens DR, Yamada KM (2001) Taking cell-matrix adhesions to the third dimension. Science 294:1708–1712

Du P, Subbiah R, Park JH, Park K (2014) Vascular morphogenesis of human umbilical vein endothelial cells on cell-derived macromolecular matrix microenvironment. Tissue Eng A:2365–2377

Du P, Suhaeri M, Ha SS, Oh SJ, Kim SH, Park K (2017) Human lung fibroblast-derived matrix facilitates vascular morphogenesis in 3D environment and enhances skin wound healing. Acta Biomater 54: 333–344

He F, Pei M (2013) Extracellular matrix enhances differentiation of adipose stem cells from infrapatellar fat pad toward chondrogenesis. J Tissue Eng Regen Med 7:73–84

Hong Y, Kim YS, Hong SH, Oh YM (2016) Therapeutic effects of adipose-derived stem cells pretreated with pioglitazone in an emphysema mouse model. Exp Mol Med 48:e266

Huh JW, Kim SY, Lee JH, Lee JS, Van Ta Q, Kim M, Oh YM, Lee YS, Lee SD (2011) Bone marrow cells repair cigarette smoke-induced emphysema in rats. Am J Phys Lung Cell Mol Phys 301:L255–L266

Kim IG, Hwang MP, Du P, Ko J, Ha CW, Do SH, Park K (2015) Bioactive cell-derived matrices combined with polymer mesh scaffold for osteogenesis and bone healing. Biomaterials 50:75–86

Kim IG, Ko J, Lee HR, Do SH, Park K (2016) Mesenchymal cells condensation-inducible mesh scaffolds for cartilage tissue engineering. Biomaterials 85:18–29

Ko JY, Lee J, Lee J, Im GI (2017) Intra-articular xenoplantation of adipose-derived stromal cells to treat osteoarthritis in a goat model. TERM 14:65–71

Korzyńska A, Zychowicz M (2008) A method of estimation of the cell doubling time on basis of the cell culture monitoring data. BBE 28: 75–82

Kucia M, Ratajczak J, Reca R, Janowska-Wieczorek A, Ratajczak MZ (2004) Tissue-specific muscle, neural and liver stem/progenitor cells reside in the bone marrow, respond to an SDF-1 gradient and are mobilized into peripheral blood during stress and tissue injury. Blood Cells Mol Dis 32:52–57

Kusuma GK, Brennecke SP, O'Connor AJ, Kalionis B, Heath DE (2017) Decellularized extracellular matrices produced from immortal cell lines derived from different parts of the placenta support primary mesenchymal stem cell expansion. PLoS One 12:e0171488

Kusuma GK, Yang MC, Brennecke SP, O'Connor AJ, Kalionis B, Heath DE (2018) Transferable matrixes produced from decellularized extracellular matrix promote proliferation and osteogenic differentiation of mesenchymal stem cells and facilitate scale-up. ACS Biomater Sci Eng. https://doi.org/10.1021/acsbiomaterials.7b00747

Lai Y, Sun Y, Skinner CM, Son EL, Lu Z, Tuan RS, Jilka RL, Ling J, Chen XD (2010) Reconstitution of marrow-derived extracellular matrix ex vivo: a robust culture system for expanding large-scale highly functional human mesenchymal stem cells. Stem Cells Dev 19:1095–1107

Lee OK, Kuo TK, Chen WM, Lee KD, Hsieh SL, Chen TH (2004) Isolation of multipotent mesenchymal stem cells from umbilical cord. Blood 103:1669–1675

Li O, Tormin A, Sundberg B, Hyllner J, Le Blanc K, Scheding S (2013) Human embryonic stem cell-derived mesenchymal stroma cells (hES-MSCs) engraft in vivo and support hematopoiesis without suppressing immune function: implications for off-the shelf ES-MSC therapies. PLoS One 8:e55319

Lin H, Yang G, Tan J, Tuan RS (2012) Influence of decellularized matrix derived from human mesenchymal stem cells on their proliferation, migration and multi-lineage differentiation potential. Biomaterials 33:4480–4489

Malgieri A, Kantzari E, Patrizi MP, Gambardella S (2010) Bone marrow and umbilical cord blood human mesenchymal stem cells: state of the art. Int J Clin Exp Med 3:248–269

Moriscot C, de Fraipont F, Richard MJ, Marchand M, Savatier P, Bosco D, Favrot M, Benhamou PY (2015) Human bone marrow mesenchymal stem cells can express insulin and key transcription factors of the endocrine pancreas developmental pathway upon genetic and/or microenvironmental manipulation in vitro. Stem Cells 23:594–603

Ng CP, Sharif AR, Heath DE, Chow JW, Zhang CB, Chan-Park MB, Hammond PT, Chan JK, Griffith LG (2014) Enhanced ex vivo expansion of adult mesenchymal stem cells by fetal mesenchymal stem cell ECM. Biomaterials 35:4046–4057

Pittenger MF, Mackay AM, Beck SC, Jaiswal RK, Douglas R, Mosca JD, Moorman MA, Simonetti DW, Craig S, Marshak DR (1990) Multilineage potential of adult human mesenchymal stem cells. Science 284:143–147

Qian L, Saltzman WM (2004) Improving the expansion and neuronal differentiation of mesenchymal stem cells through culture surface modification. Biomaterials 25:1331–1337

Rabe KF, Hurd S, Anzueto A, Barnes PJ, Buist SA, Calverley P, Fukuchi Y, Jenkins C, Rodriguez-Roisin R, van Weel C, Zielinski J (2007) Global strategy for the diagnosis, management, and prevention of chronic obstructive pulmonary disease: GOLD executive summary. Am J Respir Crit Care Med 176:532–555

Sethe S, Scutt A, Stolzing A (2006) Aging of mesenchymal stem cells. Ageing Res Rev 5:91–116

Shakouri-Motlagh A, O'Connor AJ, Brennecke SP, Kalionis B, Heath DE (2017) Native and solubilized decellularized extracellular matrix: a critical assessment of their potential for improving the expansion of mesenchymal stem cells. Acta Biomater 55:1–12

Toh WS, Lim TC, Kurisawa M, Spector M (2012) Modulation of mesenchymal stem cell chondrogenesis in a tunable hyaluronic acid hydrogel microenvironment. Biomaterials 33:3835–3845

Ueno M, Maeno T, Nishimura S, Ogata F, Masubuchi H, Hara K, Yamaguchi K, Aoki F, Suga T, Nagai R, Kurabayashi M (2015) Alendronate inhalation ameliorates elastase-induced pulmonary emphysema in mice by induction of apoptosis of alveolar macrophages. Nat Commun 6:6332

Wagner W, Horn P, Castoldi M, Diehlmann A, Bork S, Saffrich R, Benes V, Blake J, Pfister S, Eckstein V, Ho AD (2008) Replicative senescence of mesenchymal stem cells: a continuous and organized process. PLoS One 3:e2213

Wang Y, Zhang Z, Chi Y, Zhang Q, Xu F, Yang Z, Meng L, Yang S, Yan S, Mao A, Zhang J, Yang Y, Wang S, Cui J, Liang L, Ji Y, Han ZB, Fang X, Han ZC (2013) Long-term cultured mesenchymal stem cells frequently develop genomic mutations but do not undergo malignant transformation. Cell Death Dis 4:e950